Published in final edited form as:
Sci Signal. ; 5(228): ra43. doi:10.1126/scisignal.2002437.

The *lin-4* microRNA Targets the LIN-14 Transcription Factor to Inhibit Netrin-Mediated Axon Attraction

Yan Zou[1], **Hui Chiu**[1], **Dorothée Domenger**[2], **Chiou-Fen Chuang**[1,3,+], and **Chieh Chang**[1,2,3,+]

[1]Division of Developmental Biology, Cincinnati Children's Hospital Research Foundation, Cincinnati, Ohio 45229

[2]Dept. of Biology and Dept. of Neurology and Neurosurgery, McGill University, Montreal, Quebec H3A 1B1, Canada

Abstract

lin-4 (miR-125) microRNAs are deeply conserved across animal phylogeny. They are among the first microRNAs discovered and were implicated in regulating developmental timing in *C. elegans*. In this study, we report that mutations in *lin-4* microRNA specifically suppress the AVM axon guidance defects in *slt-1* mutants through enhancement of netrin attraction. *lin-4* expression in AVM neurons rescued *lin-4* mutant phenotypes in AVM axon guidance, suggesting that *lin-4* acts cell autonomously in AVM to inhibit its axon attraction to netrin. *lin-4* is expressed strongly in the AVM neuron when its axon guidance is underway, and is almost undetectable in the ALM neuron whose axon guidance is netrin independent. The transcription factor *lin-14*, a necessary target of *lin-4* microRNA in the AVM neurons, stimulates netrin-mediated AVM axon ventral guidance. *lin-14*'s positive effect in netrin attraction is mediated by the receptor *unc-40* (DCC) and its cofactor *madd-2* functioning through a combination of the *unc-34* (Ena) and *ced-10* (Rac1)-dependent downstream pathways. *lin-14* stimulates netrin-mediated axon attraction in part by enhancing UNC-40 protein expression. Our study indicates that the eventual down-regulation of *lin-14* activity in the AVM neurons at the end of axon guidance is caused by *lin-4* microRNA inhibition.

Introduction

During development of the nervous system, the *C. elegans* anterior ventral microtubule axon (AVM) is guided to the ventral midline by two cues, the UNC-6 (netrin) attractant recognized by the UNC-40 (DCC) receptor and the SLT-1 (slit) repellent recognized by the SAX-3 (robo) receptor. Upon reaching the ventral midline, the AVM axon moves anteriorly to the nerve ring (*1*), a neuropil generally viewed as the animal's brain. Axons are attracted to targets, but upon arriving they must switch their responsiveness to guidance cues at the targets such that they are no longer sensitive to axon cues but rather can proceed with synapse formation. Thus, AVM axons are less able to respond to UNC-6 (netrin) as their development advances. This developmental loss of responsiveness to the axon guidance cue, in this case netrin, might be accounted for by either extrinsic inhibitory signals or intrinsic neuronal aging.

[+]To whom correspondence should be addressed. chieh.chang@cchmc.org (C.C.); chiou-fen.chuang@cchmc.org (C.-F.C.).
[3]Senior authors contributed equally to this work.

Author contributions: Y.Z. and H.C. performed experiments and analyzed data; D.D. analyzed axonal phenotypes in *lin-4*; *slt-1* and *lin-4*; *unc-6* strains; and C.C. and C.-F.C. designed experiments, analyzed data and wrote the paper.

Competing interests: The authors declare that they do not have any competing financial, personal, or professional interest.

Founding members of the microRNA family were first described in *C. elegans* (*2*–*4*). Since then, microRNAs have been shown to be involved in such diverse events as development, metabolism, apoptosis, cell fate determination, and cancer formation. MicroRNAs down-regulate gene expression by interacting with partially complementary sequences in the 3′UTRs of their target genes (*2*, *3*). The *C. elegans* genome encodes hundreds of microRNAs, about 30% of which are conserved within animals, suggesting ancient functions (*5*). Many of the recently discovered microRNAs are spatially expressed in the nervous system, such as *lsy-6* and *mir-273* (*6*, *7*), implying an important role for microRNAs in spatial pattern formation in the nervous system. Others are temporally expressed during development of the nervous system, including *lin-4* (miR-125) and *let-7* (*8*–*10*), raising the possibility that microRNAs may regulate neuronal responsiveness to axon guidance cues. Although microRNAs have been clearly shown to specify left-right neuronal asymmetry and midbrain-hindbrain boundary (*6*, *7*, *11*), their roles in other aspects of neuronal development are largely unknown. Here, we report the first example of microRNA regulation of axon guidance during formation of neuronal circuit. We discovered an unexpected role for the *lin-4* microRNA in axon guidance through genetic analysis of a well-characterized axon guidance event, the growth of the AVM axon to the ventral midline in *C. elegans*. Our results show that *lin-4* microRNA functions as a potent and specific negative regulator of Netrin-mediated attraction, without effect on Slit-mediated repulsion, and provide strong evidence for *lin-4* functioning through the *lin-14* transcription factor in the AVM neuron to inhibit its axon attraction to Netrin. We believe, at the end of axon guidance, *lin-4* microRNA signals AVM neurons to undergo a developmental loss of responsiveness to Netrin through negative regulation of LIN-14 transcription factor, leading to down-regulation of UNC-40 receptor signaling.

Results

A microRNA pathway inhibits AVM axon ventral guidance potentially through negative regulation of *unc-6* (netrin) signaling

Dicer family of RNase III-related enzymes are responsible for processing most if not all premature microRNAs. In *C. elegans*, three nearly identical Argonaute proteins ALG-1, ALG-2, and RDE-1 were found to copurify with DCR-1 (Dicer) biochemically (*12*). Like Dicer, ALG-1 and ALG-2 are required for the maturation of microRNAs but only for a subgroup of them (*12*, *13*). To ask whether any of these microRNAs regulates axon guidance, we examined AVM axon ventral guidance in *alg-1*, *alg-2*, or *dcr-1* mutants.

AVM axon guidance provides a sensitive, powerful system for genetically probing how attractive and repulsive guidance signals are dynamically regulated during development. In *C. elegans*, ventral guidance of the AVM axon relies upon the combined action of an attractive UNC-6 (netrin) guidance cue from the ventral pole and a repulsive SLT-1 (Slit) guidance cue from the dorsal pole (Fig. 1A). Studying AVM axon guidance therefore presents an opportunity to evaluate the specific contribution of genes to either netrin or Slit guidance pathways. Because there are two parallel guidance pathways for AVM axon ventral guidance, genetic manipulations that potentiate signaling through one guidance pathway (such as ventral netrin) might suppress the defects caused by loss of the other guidance pathway (such as dorsal slit). Our analysis reveals several clues that may suggest how microRNA pathways regulate axon guidance. First, *dcr-1* mutation did not affect AVM axon ventral guidance, which may be due to a simultaneous knockout of microRNAs with opposite functions in AVM axon guidance (Fig. 1C). Second, *alg-2* mutant affected both netrin and *slt-1*-mediated axon guidance, suggesting that *alg-2* mutant effects on axon guidance may not be very specific (Fig. 1C). Third, *alg-1* mutation suppressed *slt-1* mutant phenotypes in AVM axon ventral guidance, consistent with the model that *alg-1* mutation specifically enhances netrin-mediated axon attraction, which compensates for loss-of-

function in *slt-1* (Fig. 1C). However it is formally possible that additional attractive forces are also enhanced in *alg-1*; *slt-1* mutants.

The effect of *alg-1* mutation on AVM axon guidance may be attributed to *lin-4* (miR-125) microRNA inactivation in AVM neurons

alg-1 is required for biogenesis of many microRNAs (*13*). We postulated that the maturation of one or more microRNAs that depends on *alg-1*, inhibits netrin-mediated AVM axon ventral attraction; and furthermore that this microRNA is likely to be expressed early in development in the first larval stage in order to regulate netrin-mediated AVM axon ventral attraction. Stem-loop RT-PCR was used to globally survey mature microRNA expression in *C. elegans* development. Spatial constraint of the stem-loop RT primer discriminates among related microRNAs that differ by as little as one nucleotide (*14*, Fig. 2A). Among 83 microRNAs we surveyed (Fig. 2B), including those with homologues in vertebrates, we identified 4 microRNAs (*lin-4*, *mir-71*, *mir-83*, and *mir-90*) whose abrupt initiation of expression in the first larval stage coincides with the timing of the AVM axon ventral guidance (Fig. 2B and fig. S1A). Among the 4 early-onset microRNAs we identified, only *lin-4* and *mir-90* are expressed in the AVM neurons (Fig. 3C–O and fig. S1B–D). For those early-onset microRNAs that are expressed in the AVM neurons, only maturation of *lin-4* microRNA is affected in *alg-1* mutants (Fig. 3P and fig. S1E). *lin-4* encodes a heterochronic microRNA that is temporally expressed during *C. elegans* development (*15*). The rapid increase of *lin-4* expression in L1 larvae is due to up-regulation of *lin-4* expression in many tissues including muscles, hypodermal cells, and neurons in the head, the tail, the ventral nerve cord, the anterior body, and the mid-body regions (Fig. 3B, C). *lin-4* microRNA binds to the 3′UTR of its target, *lin-14*, preventing its translation and permitting stage two of larval cell fate to occur (*8*). Mutations that reduce *lin-4* or enhance *lin-14* gene activities delay developmental timing of cells at the L1–L2 transition. These previous findings point to the possibility that *lin-4* mutation may prolong or enhance L1-stage AVM cell fate, resulting in enhancement of axon guidance signaling in AVM neurons. In our stem-loop RT-PCR assay, mature *lin-4* microRNA is almost undetectable in the embryonic stage (fig. S1A). However, its expression was dramatically increased at the first larval stage and persisted into adulthood (Fig. 2B). Similarly, a *lin-4* promoter reporter became highly expressed in the AVM neurons from the late-first larval stage onwards (Fig. 3D–O, 7A). The expression of this *lin-4* promoter reporter is much stronger in the AVM neurons, whose axon guidance is netrin dependent, than in the ALM neurons, whose axon guidance is netrin independent (Fig. 3D–O).

lin-4 microRNA is homologous to vertebrate miR-125a and miR-125b with the differences located only in the central region (Fig. 3A), a region believed to be looped out during target mRNA recognition (*16*). miR-125a and miR-125b have been previously implicated in neuronal development as they were first isolated from brain tissues in mice (*16*). Over-expression of miR-125, like *lin-4*, can specifically repress the expression of a *mec-4::GFP::lin-14 3′UTR* sensor containing seven complementary *mir-125* binding sites in the AVM neurons (fig. S2 and S3).

lin-4 microRNA inhibits *unc-6* (netrin) signaling during AVM axon guidance

The *lin-4(e912)* mutation used in this study is a loss-of-function null allele. We found that loss of *lin-4* function recapitulates the *alg-1* mutant phenotypes in AVM axon ventral guidance. *lin-4(e912)* mutation, like *alg-1* mutation, alone does not display abnormal AVM axon ventral guidance. However, *lin-4(e912)* mutation, like *alg-1* mutation, enhances netrin-mediated axon attraction, suppressing the AVM axon guidance defect in *slt-1* (slit) but not *unc-6* (netrin) null mutants (Fig. 1B, 1C, 4A, 4B). Recent studies by Culotti's group identified EVA-1 as a SAX-3 (Robo) co-receptor, which binds to SLT-1 and SAX-3 on the

cell surface (*17*). EVA-1 and SAX-3 are both required for *slt-1*-mediated AVM axon repulsion. However, different from EVA-1 being acting strictly as a SLT-1 receptor, SAX-3 (Robo) can also inhibit or silence UNC-40 (DCC) signaling in the absence of SLT-1. To further determine the specificity of *lin-4*'s function as a regulator of netrin pathway, we tested genetic interactions between *lin-4* and *eva-1* and between *lin-4* and *sax-3* null mutants. We found that *lin-4* mutation significantly suppresses *eva-1* mutant phenotypes as expected (Fig. 4B). However, *lin-4* mutation does not suppress *sax-3* mutant phenotypes (Fig. 4B). These results suggest that *lin-4*'s function in netrin-mediated AVM axon guidance depends on *sax-3* and that *lin-4* and *sax-3* may inhibit UNC-40 (DCC) signaling through a similar mechanism.

The effect of *lin-4* mutation on AVM axon guidance appears to be cell autonomous since expression of *lin-4* microRNA in AVM neurons but not body wall muscles or hypodermal cells significantly rescued the *lin-4* mutant phenotypes in suppressing AVM axon guidance defects in *slt-1* mutants (Fig. 4C). The same *mec-4::lin-4* transgene is sufficient to repress the expression of a *mec-4::GFP::lin-14 3′UTR* sensor in the AVM neurons, suggesting that the *mec-4::lin-4* transgene is functional (fig. S2). Taken together, our results indicate that depletion of *lin-4* microRNA in AVM neurons enhances netrin-mediated axon attraction, suppressing the AVM axon guidance defect in *slt-1* mutants. Thus, *lin-4* microRNA may inhibit either duration or amplitude of *unc-6* (netrin) signaling in AVM axon guidance.

It was previously shown that *lin-4* loss-of-function mutation affects PVM neuron specification (increase number by 40%) but not AVM neuron (0% increase) as judged by the *mec-7* immunocytochemistry (*18*). We also found that *lin-4* mutation does not have any noticeable effect on AVM cell fate. We analyzed many aspects of AVM neuronal development in *lin-4* mutants, including cell migration, ventral and anterior axon growth, and expression of two AVM neuronal markers *mec-4* and *mir-90* and found that none of these AVM qualities is affected by the *lin-4* mutation (Table S1). In fact, we consistently detected *lin-4* expression in the AVM neurons only after AVM already migrated to its final position along the anterior and posterior axis and started sending out axon (Fig. 7A).

lin-14, an essential target gene of *lin-4* microRNA in the AVM neurons, stimulates AVM axon ventral guidance

lin-14 encodes a transcription factor that specifies the timing and sequence of stage-specific developmental events in *C. elegans* (*19*, *20*). Since *lin-14* is expressed in the AVM neurons (Fig. 5B) and *lin-14* 3′UTR contains multiple *lin-4* binding sites, we tested if *lin-14* is subject to the negative regulation by *lin-4* microRNA in the AVM neurons. We anticipate that, if *lin-14* is the target of *lin-4* microRNA, a gain-of-function *lin-14* mutant allele (*n355gf*) that removes all seven complementary *lin-4* binding sites at *lin-14* 3′UTR would mimic a loss-of-function *lin-4* mutant allele in enhancing AVM axon ventral guidance. Our result supports this possibility by showing that *lin-14(n355gf)* mutation suppressed the AVM axon guidance defects in *slt-1* mutants to the similar caliber as *lin-4(e912lf)* mutation (Fig. 4B, 5C). While suppressing the AVM axon guidance defects in *slt-1* mutants, *lin-14(n355gf)* mutation does not suppress those in a loss-of-function *unc-40* (DCC) mutant, suggesting that *lin-14*'s function depends on DCC (Fig. 5C). Reduced *lin-14* activity suppressed *lin-4* loss-of-function phenotypes in AVM axon guidance (Fig. 5D). In fact, *lin-4*; *lin-14 slt-1* triple mutants are phenotypically indistinguishable to *lin-14 slt-1* double mutants, suggesting that *lin-14* acts downstream of *lin-4* microRNA in the same genetic pathway for AVM axon guidance (Fig. 5D). To ask if *lin-14* functions in the AVM neurons for this effect, we expressed *lin-14* in the AVM neurons using a cell-type specific promoter *mec-4* and found that, like the *lin-4* loss-of-function phenotype, overexpressing *lin-14* in the AVM neurons enhanced netrin-mediated AVM axon attraction, suppressing the defects of AVM axon guidance in *slt-1* mutants (Fig. 5E, F). This result suggests that *lin-14* likely

functions within the AVM neurons to regulate their axon ventral guidance. To further test the effect of *lin-4* microRNA on *lin-14* expression in the AVM neurons, we built two sensor constructs with either the *lin-14 3′UTR*, containing seven *lin-4* binding sites (Fig. 6A), fused to a GFP reporter or a control *3′UTR* (*unc-54*), containing no-known *lin-4* binding site, fused to a mCherry reporter, and expressed them in the AVM neurons. In L4 stage, comparing to wild-type AVM neurons, a substantially higher GFP (normalized by mCherry) signal is detected in the AVM neurons in *lin-4* mutants, suggesting that *lin-4* microRNA is necessary for down-regulation of *lin-14 3′UTR* in the AVM neurons (Fig. 6B, C). Furthermore, over-expression of *lin-4* microRNA in the AVM neurons repressed the expression of *GFP::lin-14 3′UTR* but not *GFP::unc-54 3′UTR* sensors (fig. S2), suggesting that *lin-4* microRNA is sufficient for down-regulation of *lin-14* 3′UTR in the AVM neurons.

To understand the dynamic regulation of *lin-14 3′UTR* activity during AVM axon guidance, we analyzed the expression curve of a *GFP::lin-14 3′UTR* sensor in the AVM neurons in L1 stage. We found that, over time, *lin-14 3′UTR* activity in the AVM neurons becomes lower in wild-type animals (Fig. 7B). In contrast, *lin-14 3′UTR* activity in the AVM neurons remains steady and even becomes mildly higher over time in *lin-4* mutants (Fig. 7C). These results suggest that the observed down-regulation of *lin-14 3′UTR* activity in the AVM neurons during axon guidance is caused by *lin-4* microRNA inhibition.

lin-14 is not the only known target of *lin-4* microRNA. *hbl-1* gene, the *C. elegans hunchback* ortholog, also contains two *lin-4* complementary elements at its 3′UTR and *lin-4* microRNA is required for down-regulation of *hbl-1* in the ventral nerve cord neurons (*9*, *10*). In addition, *lin-41*, a member of a large family of RBCC (ring finger, B box, coiled coil) proteins, contains one *lin-4* microRNA binding site at its 3′UTR (*21*). Over-expressing *hbl-1* or *lin-41* in the AVM neurons did not recapitulate the *lin-4* loss-of-function mutant phenotype in suppressing the AVM axon guidance defects in *slt-1* mutants, suggesting that *hbl-1* and *lin-41* are not the *lin-4* microRNA targets in regulating AVM axon ventral guidance (Fig. 5C).

lin-14's positive effect in netrin attraction is mediated by the receptor *unc-40* and its cofactor *madd-2* functioning through a combination of the *unc-34* and *ced-10*-dependent downstream pathways

MADD-2 is a cofactor for the receptor UNC-40 (DCC) and potentiates UNC-40 activity in AVM (*22*, *23*, Fig. 8). UNC-40 signaling in AVM is mediated by two downstream pathways, one involving UNC-34, an enabled (Ena) homolog, and the other CED-10, a Rac guanosine triphosphatase (*24*, *25*, Fig. 8). MIG-10, a Lamellipodin homolog, defines a downstream pathway that is partially overlapped with either UNC-34 or CED-10 (*26*–*28*). To test whether *lin-14*'s positive effect in netrin attraction is mediated by the receptor *unc-40* and its cofactor *madd-2*, we asked if *unc-40* or *madd-2* mutation could block the *lin-14* over-expression effects. *lin-14* over-expression is no longer able to suppress the AVM guidance defects in *slt-1*; *unc-40* and *slt-1*; *madd-2* double mutants (Fig. 8). These results suggest that *lin-14* effect entirely depends on *unc-40* receptor and its cofactor *madd-2*. To address whether either of the downstream pathways may mediate the *lin-14* effect, we disrupted each downstream pathway in a *slt-1* mutant background, where only *unc-40* guidance signaling is active in AVM, and asked whether the *lin-14* over-expression could still modify the AVM phenotype. The *lin-14* over-expression significantly suppressed the AVM defects of *slt-1*; *unc-34*, *slt-1*; *mig-10* and *slt-1*; *ced-10* double mutants (Fig. 8). These results suggest that the *slt-1*; *unc-34*, *slt-1*; *mig-10* and *slt-1*; *ced-10* double mutants still retain a downstream pathway that is stimulated by *lin-14*. To test whether a combination of the downstream pathways might mediate *lin-14* effect, we disrupted two downstream pathways at a time in a *slt-1* mutant background, and asked whether the *lin-14* over-expression could still modify the AVM phenotype. We noticed that wild type animals

carrying the *Pmec-4::lin-14* transgenes are sub-viable, which may explain why *slt-1*; *ced-10*; *unc-34* and *slt-1*; *mig-10*; *unc-34* triple mutants may not be viable when expressing the *Pmec-4::lin-14* transgenes. To overcome the lethality problem, we used *Pmec-7::FP4::mito* to specifically disrupt *unc-34* function only in the AVM neurons in the *slt-1*; *ced-10*; *Ex(Pmec-4::lin-14)* and *slt-1*; *mig-10*; *Ex(Pmec-4::lin-14)* strains. Expression of FP4-MITO depletes Ena (VASP) proteins from their normal subcellular locations, sequesters them on mitochondria, and neutralizes their function (*29*). In addition, we also used an RNAi approach to knockdown *ced-10* function in the *slt-1*; *unc-34*; *Ex(Pmec-4::lin-14)* strain. The *lin-14* over-expression significantly suppressed the AVM guidance defects of *slt-1*; *mig-10*; *unc-34* but not *slt-1*; *unc-34*; *ced-10* triple mutants (Fig. 8). Thus the *slt-1*; *mig-10*; *unc-34* triple mutants retain a downstream pathway that is stimulated by *lin-14*, whereas the *slt-1*; *unc-34*; *ced-10* triple mutants have lost the *lin-14*-sensitive signaling pathways. These results therefore suggest that *lin-14*'s positive effect in netrin attraction is mediated by the receptor *unc-40* and its cofactor *madd-2* functioning through a combination of the *unc-34* and *ced-10*-dependent downstream pathways.

lin-14 stimulates netrin-mediated axon attraction in part by enhancing UNC-40 protein expression

We show that over-expression of *lin-14* in the AVM neurons can suppress AVM axon ventral guidance defects in *slt-1* mutants. The effect of *lin-14* over-expression can be blocked by mutations in *unc-40*, *madd-2*, or a combination of *unc-34* and *ced-10* genes (Fig. 8). Thus, the positive effect of *lin-14* in netrin attraction is mediated by *unc-40* receptor and its cofactor *madd-2* functioning through two parallel downstream pathways *unc-34* and *ced-10* (Fig. 8). Since *madd-2*, *unc-34* and *ced-10* transduce guidance signal that is originated from the *unc-40* receptor, we wonder whether *unc-40* is the prime target of *lin-14* regulation in the netrin pathway. LIN-14 encodes a transcription factor with unknown function in neurons (*19*, *20*). To ask whether *lin-14* may affect *unc-40* promoter activity or protein expression, we analyzed the effect of *lin-14* on *unc-40* promoter activity and protein expression in the anterior touch neurons. We found that *lin-14* over-expression does not affect the expression intensity of either a 3.5-kb or a 5-kb *unc-40 promoter::GFP* reporter in the AVM neurons (fig. S4). In fact, *lin-14* did not affect the promoter activity of various *unc-40* pathway genes we analyzed (fig. S4). To determine if UNC-40 proteins can be regulated by *lin-14*, we generated three transgenic lines that express UNC-40::GFP fusion proteins in touch neurons at different amounts. Expression of UNC-40::GFP proteins at low amount in touch neurons results in 100% of cases showing UNC-40 proteins localized to the perinuclear region in vesicle-like compartments (Fig. 9A, B). Medium amount of UNC-40 expression reduces percentage of touch neurons showing restricted UNC-40 perinuclear localization and increases percentage of touch neurons with a broader UNC-40 distribution (Fig. 9B). High amount of UNC-40 expression causes 100% of AVM and ALM neurons expanding UNC-40 protein distribution to the whole cell (Fig. 9B). Interestingly, over-expression of *lin-14* can also expand UNC-40 protein distribution from the perinuclear region to the whole cell (Fig. 9A, B). Our results thus suggest that *lin-14* stimulates netrin-mediated axon attraction in part by enhancing UNC-40 protein expression. Indeed, over-expression of *unc-40::GFP* in the AVM neurons recapitulated the effect of *lin-14* over-expression, suppressing AVM axon ventral guidance defects in *slt-1* but not *unc-6* mutants (Fig. 9C).

Discussion

Roles for microRNAs in regulating neuronal development have been suggested before by the observation of defects in asymmetric neuronal development in *C. elegans* mutant in specific microRNAs, like *lsy-6* and *mir-273*, and by *in vivo* studies of neuronal

morphogenesis in vertebrate microRNA mutants (*6*, *7*, *11*), but whether microRNAs participate in axon guidance is unknown. Local translational regulation of axon guidance molecules at the developing growth cones by microRNAs has been long speculated. But our discovery here is a conceptual departure. We showed that a developmental timing microRNA represses the expression of a transcription factor to inhibit Netrin-mediated axon attraction. We believe this microRNA signals the neuron to undergo a developmental switch of responsiveness to netrin as its axon guidance comes to an end.

We discovered an unexpected role for the *lin-4* microRNA in axon guidance through genetic analysis of a well-characterized axon guidance event, the growth of the AVM axon to the ventral midline in *C. elegans*. Our results show that *lin-4* microRNA functions as a potent and specific negative regulator of Netrin-mediated attraction, without effect on Slit-mediated repulsion, and provide strong evidence that *lin-4* represses the expression of *lin-14* transcription factor in the AVM neuron to inhibit its axon attraction to Netrin. We further show that *lin-14*'s positive effect in netrin attraction is mediated by the receptor *unc-40* and its cofactor *madd-2* functioning through a combination of the *unc-34* and *ced-10*-dependent downstream pathways. In this study, we identified the molecular mechanisms by which *lin-4* regulates netrin-mediated AVM axon attraction, it remains unknown, however, what and how signal turns on *lin-4* expression in the AVM neurons.

lin-4 promoter GFP reporter is broadly expressed in *C. elegans* neurons during development of the nervous system and its expression is broader and generally stronger in the L1 stage than in the embryonic stage (Fig. 3B, C). Notably, it is expressed in lateral ganglion (ADL, AWB, AWC, AFD), ventral nerve cord (DA, DB, DD, VD), anterior-body region (SDQR), tail (PQR), touch neurons (AVM, PVM, ALM, PLM), and HSN neurons. *lin-14* promoter GFP reporter is also broadly expressed in *C. elegans* neurons. Its strong expression in neurons starts in the late embryonic stage (Fig. 5A). Analysis of expression patterns of *lin-4* and *lin-14* promoter reporters reveals overlapping expression of two genes in several neurons, including AVM, ALM, PVM, PLM, DD, VD, DA, DB, SDQR, HSN, and PQR. These results suggest that the *lin-4* and *lin-14* relationship may be extended beyond AVM neurons. Some of these neurons are known to be guided by *unc-40* alone signaling (AVM, PVM, HSN, and ADL) while others are guided by *unc-40* + *unc-5* signaling (SDQR, DD, VD, DA and DB).

While *lin-4* and *lin-14* mutations affect the timing of HSN axon outgrowth, they do not affect the timing of AVM axon outgrowth. Thus, the effect of *lin-4* and *lin-14* mutations on AVM axon guidance is likely direct and not due to the temporal decoupling of axon outgrowth and axon guidance. We analyzed HSN axon outgrowth in wild-type animals and *lin-4* loss-of-function mutants. We found that, in wild-type animals, HSN axon outgrowth was absent in L3 stage in most of cases (fig. S5A). However, axon outgrowth was observed in most of the wild-type HSN neurons in L4 and young adult stages (fig. S5A). In contrast, HSN neurons did not grow out axons in L3, L4, or young adult stage in *lin-4* loss-of-function mutants (fig. S5A). These results suggest that *lin-4* is required for HSN axon outgrowth. A similar observation has been made by a recent study in which *lin-4* was identified as an important factor that promotes HSN axon outgrowth, but whether it plays a role in HSN axon guidance is unclear (*30*, *31*).

When we determined the effects of *lin-4* loss-of-function and *lin-14* gain-of-function mutations on the timing of AVM axon outgrowth, we found that AVM axon outgrowth is not affected by either *lin-4* or *lin-14* mutations. 5 hours into L1 stage, axonal marker (*Pmec-4::GFP*) was not visible in AVM neurons in wild type, *lin-4*, and *lin-14* mutants. 7 hours into L1 stage, AVM axon outgrowth (both ventral and anterior projections) was detected in most of cases in wild type, *lin-4*, and *lin-14* mutants (fig. S5B). 10 hours into L1

stage, all strains we analyzed (wild type, *lin-4*, and *lin-14* mutants) showed 100% AVM axon outgrowth (fig. S5B). Thus, the timing of AVM axon outgrowth is not altered in *lin-4* and *lin-14* mutants. These results suggest that the effect of *lin-4* and *lin-14* mutations on AVM axon guidance is likely direct and not due to the altered timing of AVM axon outgrowth.

There is an emerging view that microRNAs are important in specifying the transition of cells from totipotency to commitment. Our results suggest that *lin-4* microRNA may signal the transition of AVM neurons from early phase of differentiation featured by responsiveness to axon guidance cues (netrin) to later phase of differentiation featured by loss of responsiveness to axon guidance cues (Fig. 5G). *lin-14* transcription factor is a *lin-4* microRNA target, stimulating netrin-mediated AVM axon guidance in part by enhancing UNC-40 protein expression. The fact that *lin-4* microRNA acts in the AVM neurons to negatively regulate netrin-mediated axon attraction suggests that *lin-4* microRNA either inhibits amplitude or restricts duration of *unc-40* (DCC) signaling in AVM neurons. Given that developmental mechanisms are frequently conserved across animal phylogeny, general rules of microRNA regulation of axon guidance in *C. elegans* are likely to be applicable in higher organisms.

Materials and Methods

Genetics and strains

C. elegans strains were cultured using standard methods (*32*). All strains were grown at 20°C unless otherwise specified. A strain list appears as Table S2.

Transgenic animals

“Germline” transformation of *C. elegans* was performed using standard techniques (*33*). For example, the *Pmec-4::lin-14* transgene was injected at 10 ng/μl along with the coinjection marker *Podr-1::rfp* at 40 ng/μl. Transgenic lines were maintained by following *Podr-1::rfp* fluorescence.

PCR fusion reaction

mec-4::lin-4 was generated by PCR fusion, in which two separate primary PCR products were fused by a secondary PCR. Template used was genomic DNA.

lin-4_G1	CTATCAAGTTATAGAGGGATCATGCTTCCGGCCTGTTCCCTG
lin-4_G1_R	CAGGGAACAGGCCGGAAGCATGATCCCTCTATAACTTGATAG
lin-4_G2	AGATCTGCTCAAACCGTCCTG
mec-4_P1	CCAAGCTTCAATACAAGCTC

Constructs

Pmec-4::lin-14 and *Pmec-4::hbl-1* were constructed by PCR amplification of genomic fragment of *lin-14* or *hbl-1*, followed by digestion with NheI and KpnI and ligation to *Pmec-4-pSM* vector. *Pmec-4::GFP::lin-14*$^{3'UTR}$ was constructed by PCR amplification of a 1.8-kb genomic fragment of *lin-14*$^{3'UTR}$, followed by digestion with EcoRI and SpeI and ligation to *Pmec-4-GFP-pSM* vector. *Plin-4::GFP* was constructed by PCR amplification of a 1.9-kb *lin-4* promoter fragment from genomic DNA, followed by digestion with FseI and XmaI and ligation to *GFP-pSM* vector. *Plin-14::GFP* was constructed by PCR amplification of a 4-kb *lin-14* promoter fragment from genomic DNA, followed by digestion with FseI and AscI and ligation to *GFP-pSM* vector. *Punc-40::GFP* was constructed by PCR amplification of either a 3.5-kb or a 5-kb *unc-40* promoter fragment from genomic DNA,

followed by digestion with FseI and AscI and ligation to *GFP-pSM* vector. *Pmadd-2::GFP* was constructed by PCR amplification of a 3-kb *madd-2* promoter fragment from genomic DNA, followed by digestion with FseI and AscI and ligation to *GFP-pSM* vector. *Pced-10::GFP* was constructed by PCR amplification of a 3-kb *ced-10* promoter fragment from genomic DNA, followed by digestion with FseI and AscI and ligation to *GFP-pSM* vector. *Pmig-10::GFP* was constructed by PCR amplification of a 3.5-kb *mig-10* promoter fragment from genomic DNA, followed by digestion with FseI and AscI and ligation to *GFP-pSM* vector. To generate *Pmec-4::mig-10::GFP*, a DNA fragment containing the *mig-10* cDNA was inserted at the 5′ end of GFP in a *GFP-pSM* vector containing a 1-kb fragment of the *mec-4* promoter between SphI and SalI sites. To generate *Pmec-4::unc-40::GFP*, a DNA fragment containing the *unc-40* cDNA was inserted at the 5′ end of GFP in a *GFP-pSM* vector containing a 1-kb fragment of the *mec-4* promoter between NheI and KpnI sites. For MosSCI experiments, *Pmec-4::unc-40::GFP* sequence was cut out of pSM using the FseI and SpeI restriction sites, and was cloned into a pCFJ151 MosSCI insertion vector (*34*) that had been modified to include a FseI site in the MCS (*35*).

lin-14_F_NheI	GCTAGCTAGCTTGTCCTTCTGCCCAATCAAG
lin-14_R_KpnI	CGGGGTACCTCTATTGTGGACCTTGAAGAG
hbl-1_F_NheI	GCTAGCTAGCGAAAAAGGATTAGTGGTCCTG
hbl-1_R_KpnI	CGGGGTACCTTATTGGTGTCTGGCTTGGTAC
lin-14$^{3'UTR}$_F_EcoRI	CGGAATTCACATCAGTCTCTTCACCCATC
lin_14$^{3'UTR}$_R_SpeI	GGACTAGTGTAAGGTTCAGAGATGCATC
lin-4_P_F_FseI	GTCTGGCCGGCCCATGTCCTGCCCATTCCGTAG
lin-4_P_R_XmaI	TCCCCCCGGGCTCATAAACCAACCAAAACTC
mig-10_P_F_FseI	GTCTGGCCGGCCGACAAGCAATCCATCATCATC
mig-10_P_R_AscI	CAGCGGCGCGCCGCATAAAAGAGCACAAATCAG
unc-34_P_F_FseI	GTCTGGCCGGCCAGCCCACCAAAATTACAGTAC
unc-34_P_R_AscI	CAGCGGCGCGCCCTGGCTCAAAAAAGTGCAATC
unc-40_P_F_FseI	CAGCGGCGCGCCCTTCTGTCGAATTATCGCATTC
unc-40_P_R_AscI	GTCTGGCCGGCCCATGGGCATTTATCATCACTG
madd-2_P_F_FseI	GTCTGGCCGGCCTTTCCGTGCGGTTGCTTAGAG
madd-2_P_R_AscI	CAGCGGCGCGCCTTGAGTATTGTCAGGTGGAAG
ced-10_P_F_FseI	GTCTGGCCGGCCACCGTATCCAATGGGAGCTTC
ced-10_P_R_AscI	CAGCGGCGCGCCGAGCTCCGCGAGCACAAGCAC

Stem-loop reverse transcription-PCR

We quantified the mature *lin-4* microRNA level by modifying the microRNA assay developed previously (*14*). Reverse transcription reactions contained purified total RNA, 50 nM stem-loop RT primer, 1X RT first strand buffer, 0.25 mM each of dNTPs, 10 mM $MgCl_2$, 0.1 M DTT, 200 U SuperScript III reverse transcriptase and 40 U RNase inhibitor. The mixture of RNA template, dNTPs and RT primer was incubated for 5 min at 65°C. The mixture was then placed on ice for at least 1 min before adding RT buffer, DTT, $MgCl_2$, SuperScript III and RNase inhibitor. The reaction was incubated for 50 min at 50°C before heat inactivation at 85°C for 5 min. PCR was conducted using 0.25μl RT products as template in 20μl PCR for 17 cycles.

RT_primer_lin-4	CTCAACTGGTGTCGTGGAGTCGGCAATTCAGTTGAGTCACACTT
RT_lin-4_F	CGGCGGTCCCTGAGACCTCAA
Universal reverse primer	CTGGTGTCGTGGAGTCGGCAATTC

actin-F	AATTGATGTTCGTCGTGGACTC
actin-R	TCTGAAGTCTCCCATCACTGAG

MosSCI integrations

Mos single-copy integrants were generated using the direct insertion protocol described in Frokjaer-Jensen et al. (2008). 50 EG4322 *ttTi5605*; *unc-119(ed3)* worms were injected with *rab-3::mCherry*, *myo-2::mCherry*, *myo-3::mCherry*, pJL43.1 (a vector containing the Mos1 transposase under the control of the germline promoter *glh-2*), and a vector containing the *mec-4 promoter::unc-40::GFP* sequence to be inserted flanked by sequences homologous to the insertion site. Animals that were rescued for the *unc-119* phenotype (array-positive) were allowed to starve out twice, and then *unc-119* rescued animals that lacked the three mCherry coinjection markers (integrant-positive, array negative) were cloned out from separate plates to find independent integrated lines. These lines were outcrossed twice to wild-type animals, and the presence of the intact insertion was verified by PCR.

Microscopy

Axonal processes of AVM neurons were visualized with the integrated *mec-4::gfp* transgene *zdIs5* at L4 stage. The observer was not blind to the genotype. Animals were placed on 5% Noble Agar pads in M9 buffer containing 10 mM sodium azide and examined with a Plan-NEOFLUAR 40x, 1.4 NA oil-immersion objective on a Zeiss AxioImager. Images for axons and body morphology were captured using a Zeiss Axio camera. Fluorescence intensity was measured using the Zeiss Axiovision Rel 4.7 image analysis software.

Supplementary Material

Refer to Web version on PubMed Central for supplementary material.

Acknowledgments

We thank F. Ciamacco, B. Bayne, and K. Campbell for technical assistance; We also thank B. Lesch for the MosSCI technique, A. Fire for *C. elegans* vectors, the *C. elegans* Genetic Center for *C. elegans* strains, and the WormBase for readily accessible information; V. Cleghon for critical reading of the manuscript; and C. Bargmann, M. Tessier-Lavigne, V. Ambros, and members of the Chang and Chuang labs for helpful discussions. This work was funded by grants from the following: the Whitehall Foundation Research Awards (C.C. and C.-F.C.), the March of Dimes Foundation Research Award (C.C.), the Alfred P. Sloan Research Fellowship (C.-F.C.), and the CIHR grant RMF-82501 (C.C.).

References

1. Chang C, Yu TW, Bargmann CI, Tessier-Lavigne M. Inhibition of netrin-mediated axon attraction by a receptor protein tyrosine phosphatase. Science. 2004; 305:103–106. [PubMed: 15232111]
2. Lee RC, Feinbaum RL, Ambros V. The C. elegans heterochronic gene lin-4 encodes small RNAs with antisense complementarity to lin-14. Cell. 1993; 75:843–854. [PubMed: 8252621]
3. Wightman B, Ha I, Ruvkun G. Posttranscriptional regulation of the heterochronic gene lin-14 by lin-4 mediates temporal pattern formation in C. elegans. Cell. 1993; 75:855–862. [PubMed: 8252622]
4. Reinhart BJ, Slack FJ, Basson M, Pasquinelli AE, Bettinger JC, Rougvie AE, Horvitz HR, Ruvkun G. The 21-nucleotide let-7 RNA regulates developmental timing in Caenorhabditis elegans. Nature. 2000; 403:901–906. [PubMed: 10706289]
5. Ruvkun G. The perfect storm of tiny RNAs. Nat Med. 2008; 14:1041–1045. [PubMed: 18841145]
6. Johnston RJ, Hobert O. A microRNA controlling left/right neuronal asymmetry in Caenorhabditis elegans. Nature. 2003; 426:845–849. [PubMed: 14685240]

7. Chang S, Johnston RJ Jr, Frokjaer-Jensen C, Lockery S, Hobert O. MicroRNAs act sequentially and asymmetrically to control chemosensory laterality in the nematode. Nature. 2004; 430:785–789. [PubMed: 15306811]
8. Boehm M, Slack F. A developmental timing microRNA and its target regulate life span in C. elegans. Science. 2005; 310:1954–1957. [PubMed: 16373574]
9. Abrahante JE, Daul AL, Li M, Volk ML, Tennessen JM, Miller EA, Rougvie AE. The Caenorhabditis elegans hunchback-like gene lin-57/hbl-1 controls developmental time and is regulated by microRNAs. Dev Cell. 2003; 4:625–637. [PubMed: 12737799]
10. Lin SY, Johnson SM, Abraham M, Vella MC, Pasquinelli A, Gamberi C, Gottlieb E, Slack FJ. The C. elegans hunchback homolog, hbl-1, controls temporal patterning and is a probable microRNA target. Dev Cell. 2003; 4:639–650. [PubMed: 12737800]
11. Giraldez AJ, Cinalli RM, Glasner ME, Enright AJ, Thomson JM, Baskerville S, Hammond SM, Bartel DP, Schier AF. MicroRNAs regulate brain morphogenesis in zebrafish. Science. 2005; 308:833–838. [PubMed: 15774722]
12. Duchaine TF, Wohlschlegel JA, Kennedy S, Bei Y, Conte D Jr, Pang K, Brownell DR, Harding S, Mitani S, Ruvkun G, Yates JR 3rd, Mello CC. Functional proteomics reveals the biochemical niche of C. elegans DCR-1 in multiple small-RNA-mediated pathways. Cell. 2006; 124:343–354. [PubMed: 16439208]
13. Grishok A, Pasquinelli AE, Conte D, Li N, Parrish S, Ha I, Baillie DL, Fire A, Ruvkun G, Mello CC. Genes and mechanisms related to RNA interference regulate expression of the small temporal RNAs that control C. elegans developmental timing. Cell. 2001; 106:23–34. [PubMed: 11461699]
14. Chen C, Ridzon DA, Broomer AJ, Zhou Z, Lee DH, Nguyen JT, Barbisin M, Xu NL, Mahuvakar VR, Andersen MR, Lao KQ, Livak KJ, Guegler KJ. Real-time quantification of microRNAs by stem-loop RT-PCR. Nucleic Acids Res. 2005; 33:e179. [PubMed: 16314309]
15. Banerjee D, Slack F. Control of developmental timing by small temporal RNAs: a paradigm for RNA-mediated regulation of gene expression. Bioessays. 2002; 24:119–129. [PubMed: 11835276]
16. Lagos-Quintana M, Rauhut R, Yalcin A, Meyer J, Lendeckel W, Tuschl T. Identification of tissue-specific microRNAs from mouse. Curr Biol. 2002; 12:735–739. [PubMed: 12007417]
17. Fujisawa K, Wrana JL, Culotti JG. The slit receptor EVA-1 coactivates a SAX-3/Robo mediated guidance signal in C. elegans. Science. 2007; 317:1934–1938. [PubMed: 17901337]
18. Mitani S, Du H, Hall DH, Driscoll M, Chalfie M. Combinatorial control of touch receptor neuron expression in Caenorhabditis elegans. Development. 1993; 119:773–783. [PubMed: 8187641]
19. Ruvkun G, Giusto J. The Caenorhabditis elegans heterochronic gene lin-14 encodes a nuclear protein that forms a temporal developmental switch. Nature. 1989; 338:313–319. [PubMed: 2922060]
20. Hristova M, Birse D, Hong Y, Ambros V. The Caenorhabditis elegans heterochronic regulator LIN-14 is a novel transcription factor that controls the developmental timing of transcription from the insulin/insulin-like growth factor gene ins-33 by direct DNA binding. Mol Cell Biol. 2005; 25:11059–11072. [PubMed: 16314527]
21. Slack FJ, Basson M, Liu Z, Ambros V, Horvitz HR, Ruvkun G. The lin-41 RBCC gene acts in the C. elegans heterochronic pathway between the let-7 regulatory RNA and the LIN-29 transcription factor. Mol Cell. 2000; 5:659–669. [PubMed: 10882102]
22. Hao JC, Adler CE, Mebane L, Gertler FB, Bargmann CI, Tessier-Lavigne M. The tripartite motif protein MADD-2 functions with the receptor UNC-40 (DCC) in Netrin-mediated axon attraction and branching. Dev Cell. 2010; 18:950–960. [PubMed: 20627077]
23. Alexander M, Selman G, Seetharaman A, Chan KK, D'Souza SA, Byrne AB, Roy PJ. MADD-2, a homolog of the Opitz syndrome protein MID1, regulates guidance to the midline through UNC-40 in Caenorhabditis elegans. Dev Cell. 2010; 18:961–972. [PubMed: 20627078]
24. Lundquist EA, Reddien PW, Hartwieg E, Horvitz HR, Bargmann CI. Three C. elegans Rac proteins and several alternative Rac regulators control axon guidance, cell migration and apoptotic cell phagocytosis. Development. 2001; 128:4475–4488. [PubMed: 11714673]
25. Gitai Z, Yu TW, Lundquist EA, Tessier-Lavigne M, Bargmann CI. The netrin receptor UNC-40/DCC stimulates axon attraction and outgrowth through enabled and, in parallel, Rac and UNC-115/AbLIM. Neuron. 2003; 37:53–65. [PubMed: 12526772]

26. Chang C, Adler CE, Krause M, Clark SG, Gertler FB, Tessier-Lavigne M, Bargmann CI. MIG-10/lamellipodin and AGE-1/PI3K promote axon guidance and outgrowth in response to slit and netrin. Curr Biol. 2006; 16:854–862. [PubMed: 16618541]
27. Quinn CC, Pfeil DS, Chen E, Stovall EL, Harden MV, Gavin MK, Forrester WC, Ryder EF, Soto MC, Wadsworth WG. UNC-6/netrin and SLT-1/slit guidance cues orient axon outgrowth mediated by MIG-10/RIAM/lamellipodin. Curr Biol. 2006; 16:845–853. [PubMed: 16563765]
28. Quinn CC, Pfeil DS, Wadsworth WG. CED-10/Rac1 mediates axon guidance by regulating the asymmetric distribution of MIG-10/lamellipodin. Curr Biol. 2008; 18:808–813. [PubMed: 18499456]
29. Goh KL, Cai L, Cepko CL, Gertler FB. Ena/VASP proteins regulate cortical neuronal positioning. Curr Biol. 2002; 12:565–569. [PubMed: 11937025]
30. Olsson-Carter K, Slack FJ. A developmental timing switch promotes axon outgrowth independent of known guidance receptors. PLoS Genet. 2010; 6:e1001054. [PubMed: 20700435]
31. Olsson-Carter K, Slack FJ. The POU transcription factor UNC-86 controls the timing and ventral guidance of Caenorhabditis elegans axon growth. Dev Dyn. 2011; 240:1815–1825. [PubMed: 21656875]
32. Brenner S. The genetics of Caenorhabditis elegans. Genetics. 1974; 77:71–94. [PubMed: 4366476]
33. Mello C, Fire A. DNA transformation. Methods Cell Biol. 1995; 48:451–482. [PubMed: 8531738]
34. Frokjaer-Jensen C, Davis MW, Hopkins CE, Newman BJ, Thummel JM, Olesen SP, Grunnet M, Jorgensen EM. Single-copy insertion of transgenes in Caenorhabditis elegans. Nat Genet. 2008; 40:1375–1383. [PubMed: 18953339]
35. Lesch BJ, Bargmann CI. The homeodomain protein hmbx-1 maintains asymmetric gene expression in adult *C. elegans* olfactory neurons. Genes Dev. 2010; 24:1802–1815. [PubMed: 20713521]

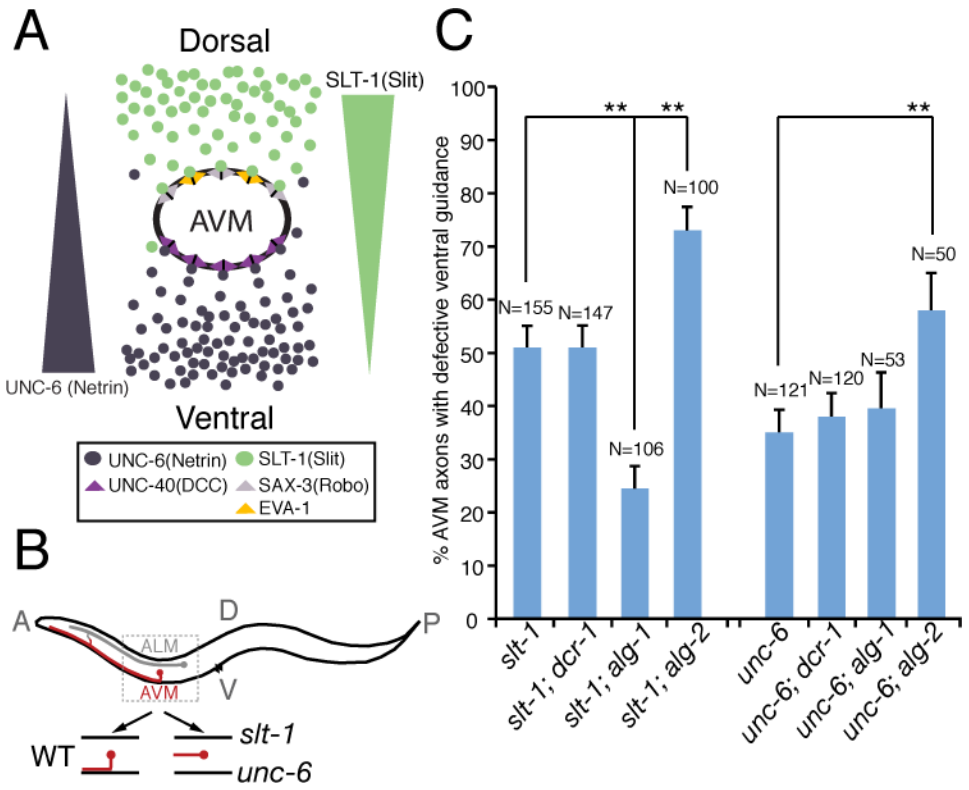

Fig. 1. Elimination of *alg-1* enhances netrin-dependent axon attraction, suppressing AVM axon ventral guidance defects in *slt-1* mutants

(A) Schematic drawing highlights signaling pathways that influence AVM axon ventral guidance in development. (B) Schematic diagram of wild-type and mutant AVM axons. (C) *alg-1* mutation specifically suppressed AVM axon ventral guidance defects in *slt-1* (slit) but not *unc-6* (netrin) mutants. *alg-1(gk214)* and *alg-2(ok304)* used in this study are null alleles. *dcr-1(mg375)* is a reduction-of-function allele. Error bars represent standard error of the proportion. Asterisks and brackets represent $P < 0.001$ by *Z*-test for two proportions.

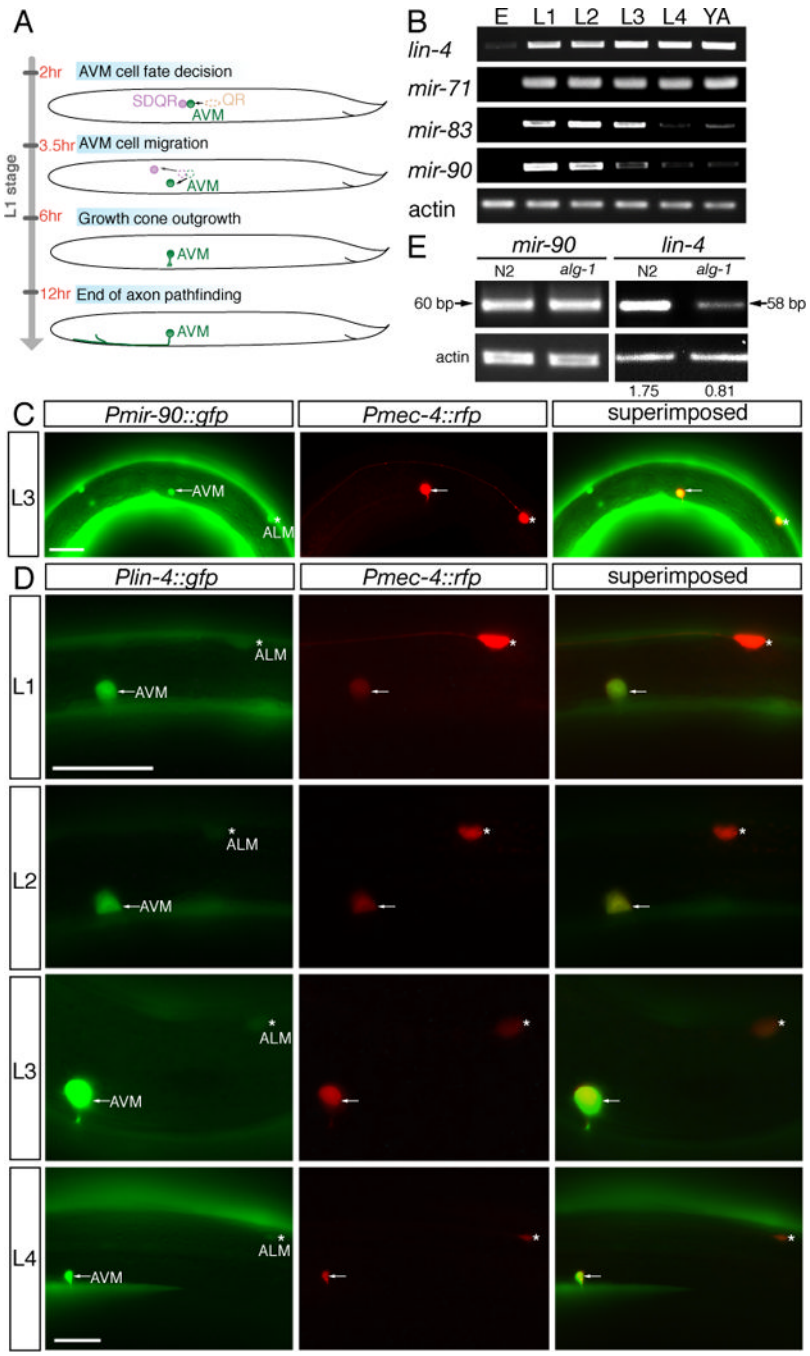

Fig. 2. Global survey of microRNA expression in *C. elegans* development

(A) Quantification of microRNAs involves two steps, stem-loop RT and conventional PCR. The stem-loop RT primer binds to the 3′ portion of the mature microRNA and is reverse transcribed with reverse transcriptase. Subsequently, the RT product is quantified using conventional PCR that includes a microRNA-specific forward primer and an universal reverse primer. The forward primer is tailed at 5′ end to increase Tm. (B) Stem-loop RT-PCR analysis of RNA isolated from populations of staged animals. Equal amount of RNA preparation from staged N2 animals was used in the RT-PCR amplification of microRNA and actin transcripts. E, L1, L2, L3, L4, and YA indicate embryonic, the first larval, the

second larval, the third larval, the forth larval, and the young adult stages, respectively. MicroRNAs were clustered based on timing of their half-maximal expression.

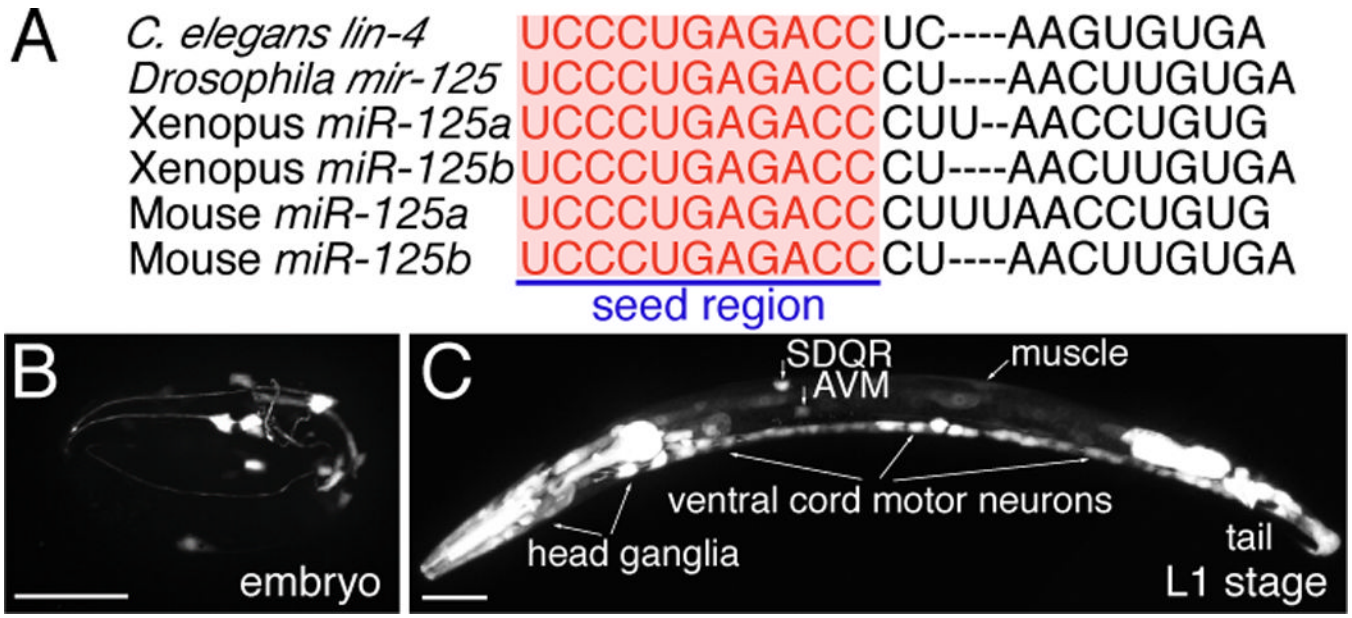

Fig. 3. Fluorescent protein promoter reporters for identifying neuronal expression of *lin-4* and stem-loop RT-PCR for detecting specifically the mature *lin-4* microRNA

(A) Sequence alignment of *C. elegans lin-4* microRNA with *Drosophila melanogaster* miR-125, Xenopus miR-125a and miR-125b, and Mouse miR-125a and miR-125b. Letters in red highlight identical sequences at the 5′ seed region, which is important for target mRNA recognition. (B–O) Expression of *lin-4* microRNA in neurons. (B) A late embryo. (C) A late L1-stage animal, whole body. Anterior body in a late L1-stage animal (D–F), a L2-stage animal (G–I), a L3-stage animal (J–L), and a L4-stage animal (M–O). A 1.9-kb *lin-4* promoter drives GFP expression in the distinct cells (B, C, D, G, J, and M). Limited *lin-4* expression in the late embryonic stage in a few head neurons. Broader *lin-4* expression in the late L1 stage in many neurons in the head, the body, and the tail. *mec-4::dsred* reporter was used to label the AVM neurons (E, H, K, and N). The superimposed images identify the GFP expressing cells as the AVM neurons (F, I, L, and O). Asterisk indicates the ALM neuron. Anterior is to left, dorsal up. Scale bar, 20 μm. (P) Measuring mature *lin-4* microRNA level by stem-loop RT-PCR in *alg-1* mutants versus wild-type (N2) animals. Equal amount of RNA preparation from either N2 or *alg-1* mutants was used in the stem-loop RT-PCR reaction for amplifying *lin-4* transcripts. Comparable amounts of actin transcripts amplified from the same RNA preparations from N2 and *alg-1* mutants serve as an internal control. Value shown above each lane indicates amount of *lin-4* normalized by actin.

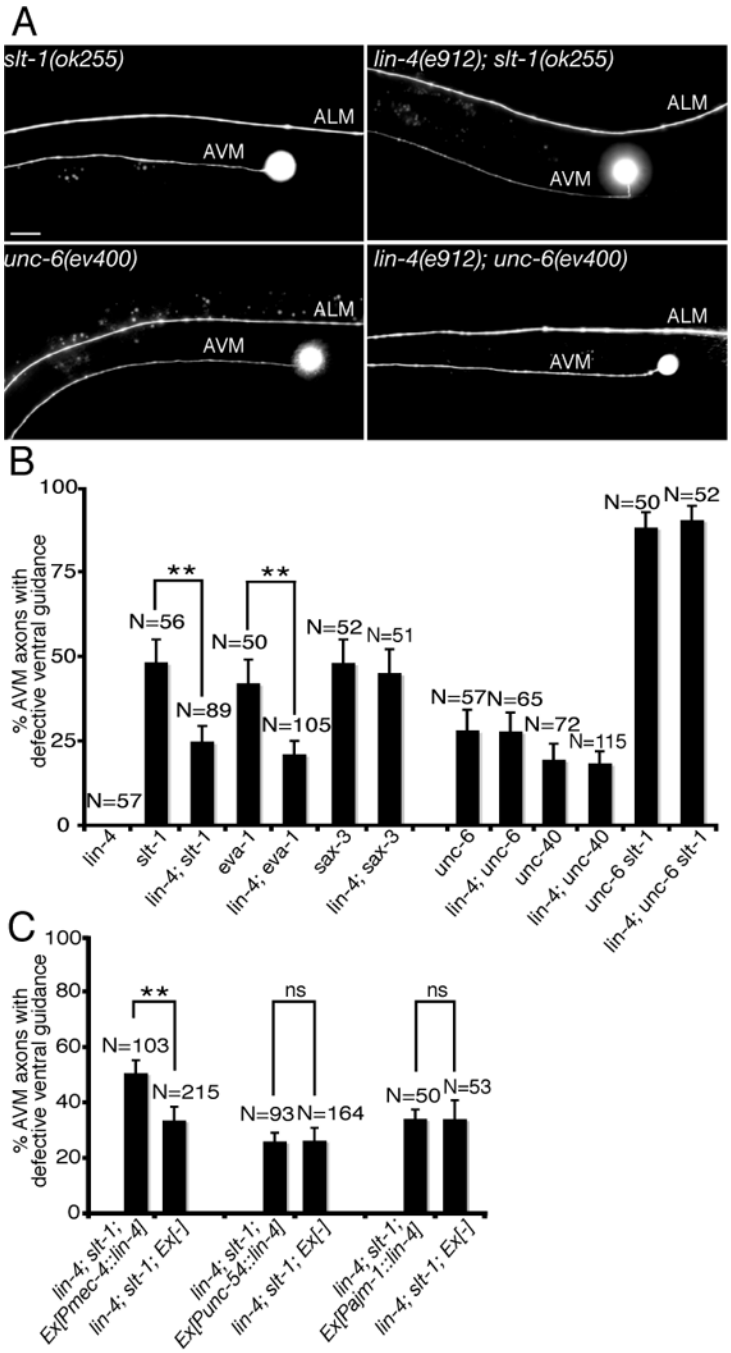

Fig. 4. Enhancing netrin-mediated axon attraction by a *lin-4* microRNA mutation

(A) Specific rescue of AVM axon guidance defects in *slt-1* mutants by a loss-of-function *lin-4* microRNA mutation. Anterior is to left, dorsal up. Scale bar, 20 μm. (B) Mutation in *lin-4* microRNA specifically suppressed AVM axon ventral guidance defects in *slt-1* (slit) and *eva-1* but not *unc-6* (netrin) and *unc-40* (DCC) mutants. Error bars represent standard error of the proportion. Asterisks indicate that comparisons between *slt-1* and *lin-4*; *slt-1* and between *eva-1* and *lin-4*; *eva-1* are significantly different at $P < 0.01$ by *Z*-test for two proportions. (C) Cell-autonomous rescue of *lin-4* mutant phenotypes in AVM axon guidance by a *mec-4::lin-4* transgene. *unc-54* and *ajm-1* promoters were used to drive *lin-4* expression in body wall muscles and hypodermal cells, respectively. Asterisks indicate that comparison

is significantly different between *lin-4*; *slt-1* with and without *mec-4::lin-4* transgene at $P < 0.01$ by *Z*-test for two proportions.

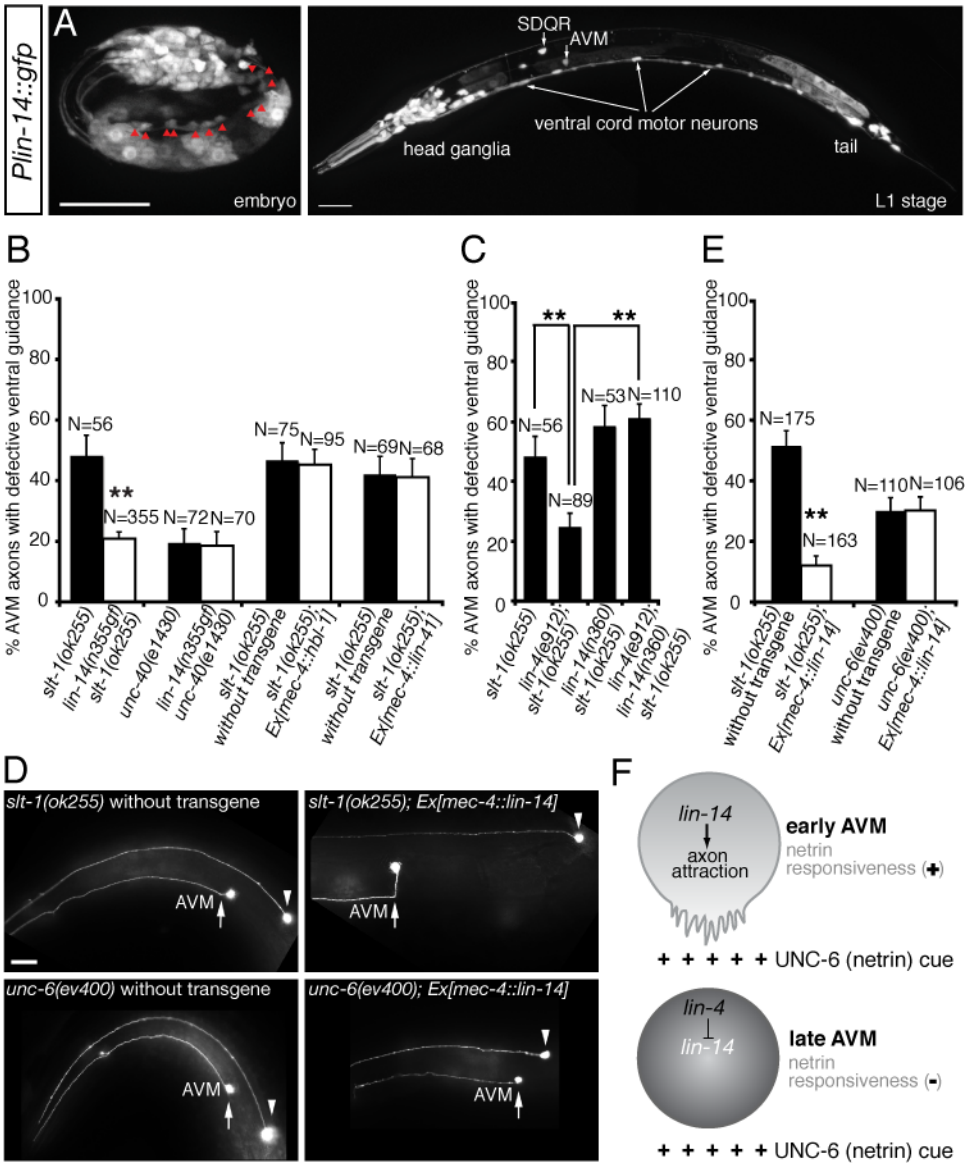

Fig. 5. The transcription factor *lin-14* enhances netrin-mediated axon attraction

(A, B) Expression of *lin-14* in neurons. (A) A late embryo. Red arrowheads indicate ventral cord motor neurons. (B) A late L1-stage animal. Scale bar, 20 μm. (C) A gain-of-function *lin-14* mutant allele (*n355gf*) recapitulates *lin-4* loss-of-function phenotype in enhancing AVM axon ventral guidance. (D) Reduced *lin-14* activity suppresses *lin-4* loss-of-function phenotype in AVM axon ventral guidance. (E) Specific rescue of AVM axon guidance defects in *slt-1* mutants by overexpressing *lin-14* in the AVM neurons. Anterior is to left, dorsal up. Scale bar, 20 μm. (F) A cell-type specific promoter-driven *lin-14* expression in the AVM neurons can enhance netrin-dependent attraction, suppressing ventral guidance defects in *slt-1* mutants. In all figures, error bars represent standard error of the proportion. Asterisks represent $P < 0.01$ by *Z*-test for two proportions. (G) Model of developmental switch of responsiveness to netrin by *lin-4* microRNA. netrin stimulates axon attraction in early AVM neurons through the transcription factor *lin-14*. *lin-4* microRNA expressed in later AVM neurons stops netrin-mediated axon attraction through inhibition of *lin-14* expression.

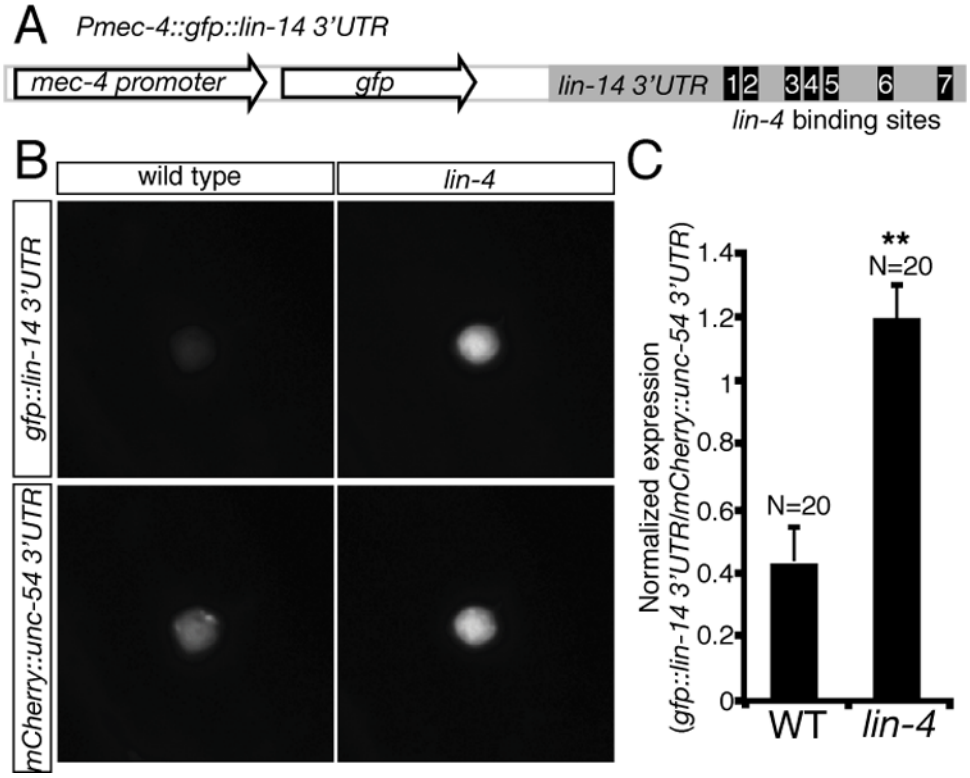

Fig. 6. Down-regulation of *lin-14 3′UTR* by endogenous *lin-4* microRNA in the AVM neurons

(A) Organization of *Pmec-4::GFP::lin-14* 3′UTR sensor construct. Seven *lin-4* microRNA binding sites were computationally predicted in the *lin-14* 3′UTR. Sensor constructs were injected at 1ng μl^{-1}. (B) Representative animals express a sensor with either the *lin-14* 3′UTR or a control (*unc-54*) 3′UTR. (C) Quantification of sensor expression in AVM neurons. The fluorescent intensity of *Pmec-4::GFP::lin-14* 3′UTR sensor is normalized by *Pmec-4::mCherry::unc-54* 3′UTR. When repression of a *lin-14* 3′UTR sensor by *lin-4* occurs, a substantially higher GFP (normalized by mCherry) signal is detected in the AVM neurons in *lin-4* mutants. Error bars indicate the s.e.m. Asterisks represent $P < 0.001$ by Student's t-Test.

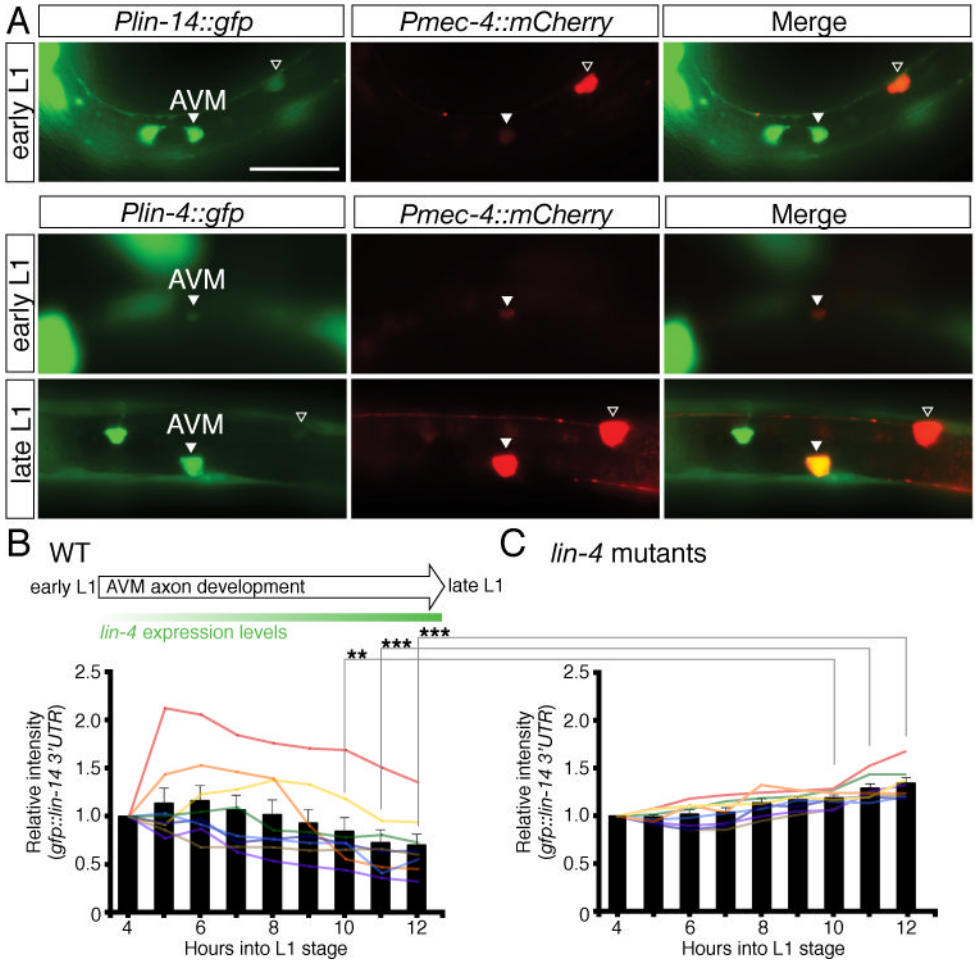

Fig. 7. Dynamic regulation of *lin-14 3′UTR* activity during AVM axon guidance in the L1 stage

(A) Temporal expression of *Plin-14::GFP* and *Plin-4::GFP* reporters in the AVM neurons. An early L1-stage animal (top panel) showing *lin-14* strongly expressed in AVM. An early L1-stage animal (middle panel) showing *lin-4* weakly expressed in AVM and a late L1-stage animal (lower panel) showing *lin-4* strongly expressed in AVM. The *Pmec-4::mCherry* reporter was used to label the AVM neurons. The merged images identify the GFP expressing cells as the AVM neurons. Arrowhead indicates the AVM neuron and the open arrowhead marks the ALM neuron. Anterior is to left, dorsal up. Scale bar, 20 μm. The expression intensity of the *GFP::lin-14 3′UTR* sensor in the AVM neurons was measured every hour at the first larval stage, starting at 4 hours after hatching and ending at 12 hours after hatching, in wild-type animals (B) and *lin-4* mutants (C). Eight animals each were measured for wild type and *lin-4* mutants. Bars represent the average intensity. ** and *** indicate intensity between wild type and *lin-4* mutants is significantly different at $P < 0.01$ and $P < 0.001$, respectively. P values were calculated using a Student's t-Test.

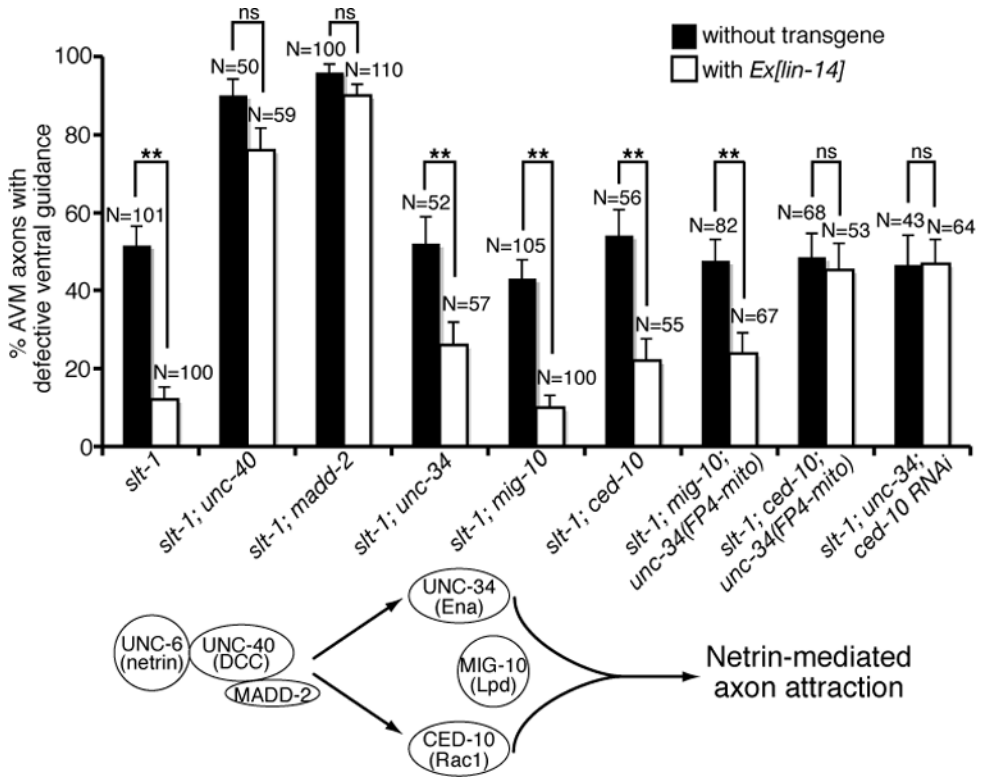

Fig. 8. *lin-14* functions through *unc-40, madd-2, unc-34* and *ced-10* to promote netrin-mediated AVM axon ventral guidance

LIN-14 requires UNC-40, MADD-2, UNC-34 and CED-10 to stimulate netrin signaling. AVM was visualized with *zdIs5[mec-4::gfp].* Asterisks indicate data significantly different from *Ex[lin-14](-)* controls ($P < 0.001$ by Z-test for two proportions).

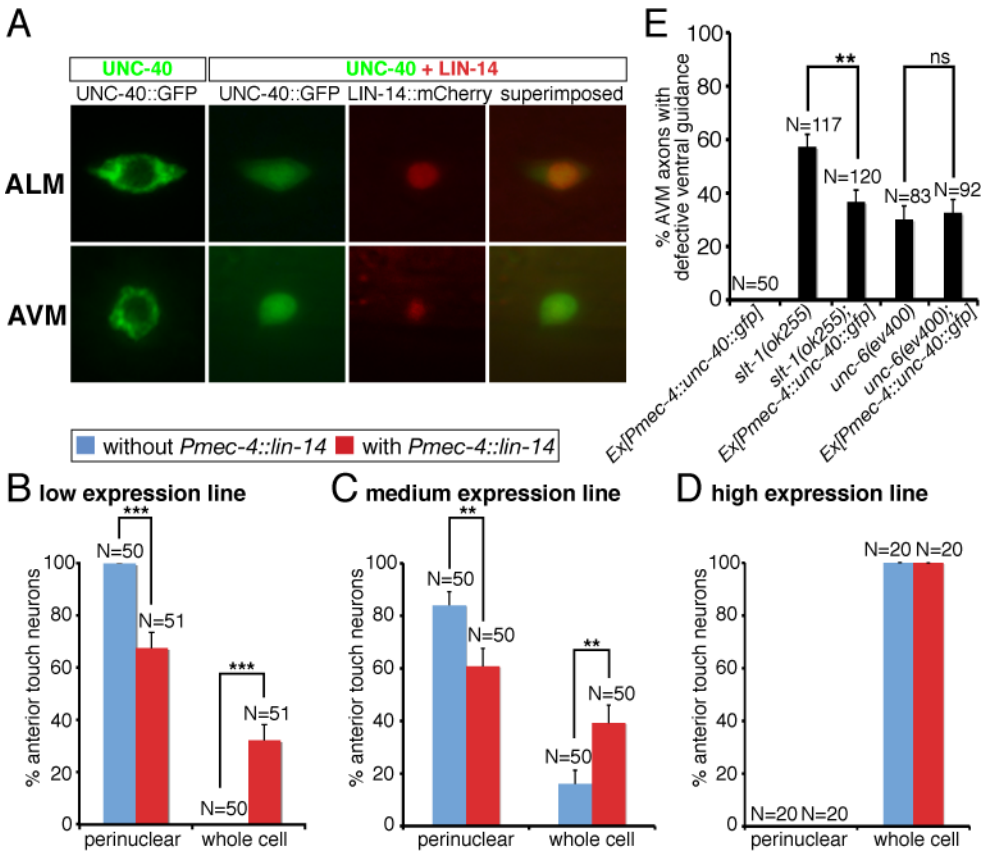

Fig. 9. Effects of *lin-14* on *unc-40* protein distribution in the anterior touch neurons

(A) Distribution of UNC-40::GFP and LIN-14::mCherry fusion proteins in the ALM and AVM neurons. (B) Quantification of anterior touch neurons showing UNC-40 protein distribution either restricted to the perinuclear region or expanded to the whole cell, depending on UNC-40 dosage and LIN-14 amount. Using the expression intensity of the *Mos[Pmec-4::unc-40::GFP]* single copy insertion line as a reference, we estimated 1 copy is the low expression line, 1.2 copies is the medium expression line, and 9.5 copies is the high expression line. (C) Over-expression of *unc-40::GFP* in the AVM neurons suppressed the AVM axon ventral guidance defects in *slt-1* but not *unc-6* mutants. In all figures, error bars represent standard error of the proportion. Asterisks and brackets represent $P < 0.01$ by *Z*-test for two proportions.